JOURNAL OF GEOPHYSICAL RESEARCH, VOL. 103, NO. A9, PAGES 20,435–20,447, SEPTEMBER 1, 1998

Dst index prediction using data-derived analogues of the magnetospheric dynamics

A. J. Klimas

NASA Goddard Space Flight Center, Greenbelt, Maryland

D. Vassiliadis

Universities Space Research Association, Seabrook, Maryland

D. N. Baker

Laboratory for Atmospheric and Space Physics, University of Colorado, Boulder

Abstract. The method of *Klimas et al.* [1997] for constructing dynamical analogues of physical input-output systems is generalized. Higher-order analogues with sensitivity to more features of the input data are derived. Solar wind VB_s parameter data are used for input and Dst index data are used for output to construct analogues of the magnetospheric dynamics responsible for Dst storms. A detailed study of the dynamics involved in a single storm is presented. It is shown that the relationship between VB_s input and Dst output for this storm can be described in the context of the model of *Burton et al.* [1975] but with variable decay time and strength of coupling to the solar wind VB_s parameter. During the storm recovery it is found that the decay time varies from $\approx$ 4 hours at the storm maximum to $\approx$ 20 hours midway in the recovery and then back to $\approx$ 10 hours. There appears to be nothing in the simultaneous solar wind data to explain this reversal in the evolution of the decay time. It is shown that the strength of coupling to the solar wind VB_s parameter varies considerably. The coupling strength peaks strongly at the time of the storm maximum and decays to low values during the storm recovery. Solar wind VB_s input during the storm recovery does not affect the recovery rate. Using this storm data, empirical nonlinear analogues are constructed. These analogues are tested out of sample for their prediction effectiveness. Comparisons with the predictions of the model due to Burton et al. are given. It is shown that these analogues are promising prediction tools, but their lack of sensitivity to solar wind dynamic pressure must be corrected.

1. Introduction

Burton et al. [1975] have introduced an effective empirical model of the Dst index response to certain parameters of the solar wind at the dayside magnetopause. In their model the contribution to Dst from the disturbed ring current is given by $Dst_0 = Dst - b\sqrt{P} + c$, which satisfies

$$\frac{dDst_0}{dt} + \frac{Dst_0}{\tau} = F(E) \tag{1}$$

in which

$$F(E) = \begin{cases} 0 & E_y < 0.5 \text{ mV/m} \\ \beta(E_y - 0.5) & E_y > 0.5 \text{ mV/m} \end{cases} \tag{2}$$

The quantity P is the solar wind dynamic pressure, and E_y is the dawn-dusk component of the solar wind electric field. The constant c is the contribution of the quiet time magnetopause and ring currents, b is the proportionality constant between the square root of the solar wind dynamic pressure and the contribution of the magnetopause currents, τ is an average timescale for the relaxation of the ring current in the absence of $F(E)$, and β is a constant that measures the strength of the magnetospheric coupling of solar wind input to Dst response. In addition, Burton et al. introduced a time shift to account for the response time of the magnetosphere and they also filtered out the high-frequency content of the input E_y.

Burton et al. [1975] fixed the constants c, b, τ, and β empirically using ground-based magnetometer data and simultaneous interplanetary solar wind data from seven storm intervals containing 10 geomagnetic storms. These are global parameters whose empirical values give the best measure of their respective roles in the model over a large time interval containing all phases of storm activity and many combinations of input to output response. As a direct consequence, the Burton et al. model, as expressed by (1), is a linear model. In addition, it is a first-order model (in derivatives) and it contains only a single timescale, the decay timescale τ.

Klimas et al. [1997] (hereinafter referred to as KEA) have recently introduced a method for constructing analogues of physical systems that accept input time series data to produce output time series data. They developed the method while studying the magnetospheric coupling of the solar wind VB_s parameter input

Paper number 98JA01559.
0148–0227/98/98JA-01559$09.00

(F(E) in (2) with the 0.5 mV/m offset removed) to the Dst index output. Their method can be viewed as an extension of the model construction method employed by *Burton et al.* [1975]. The KEA method is also empirical, but its dependence on the input and output data is local in time rather than global. As a consequence, analogues are constructed in which the parameters that enter are either expressed as (1) local parameters which are an expression of the immediate storm activity and solar wind input, or as (2) global functions of the input and output variables rather than global constants as in the Burton et al. model. Consequently, the analogues have the form of the Burton et al. model, they are expressed as ordinary differential equations for Dst, but they are generally nonlinear and expressed as higher-order differential equations containing more than one timescale in their solutions.

The method of KEA is based on the local-linear prediction model. The prediction model can be expressed as an autoregressive moving average (ARMA) filter expression [*Vassiliadis et al.*, 1995, 1996]

$$O(t+\Delta t) = \sum_{n=0}^{m-1} A_n\, O(t - n\,\Delta t) + \sum_{n=0}^{l-1} B_n\, I(t - n\,\Delta t) \quad (3)$$

for an input time series $I(t)$ and an output time series $O(t)$. This filter expression is linear but the relationship of input to output may be nonlinear. Consequently, this linear form is assumed valid only locally while nonlinearity is accounted for by allowing the filter coefficients $A_n(t)$ and $B_n(t)$ to vary in time. In applications of this method [*Vassiliadis et al.*, 1995, 1996; *Valdivia et al.*, 1996] the filter coefficients have generally been computed at every time step in a prediction run. The result is a large collection of filter coefficients. Attempts to find physical interpretations of the filter coefficients and their evolution have been largely unsuccessful.

We extend the method of KEA to map the filter relation (3) to the analogue

$$\frac{d^m O}{dt^m} + \alpha_{m-1}\frac{d^{m-1}O}{dt^{m-1}} + \cdots + \alpha_0 O = \sum_{n=0}^{l-1} \beta_n \frac{d^n I}{dt^n} \quad (4)$$

for arbitrary values of m and l; the results of KEA were limited to the single value $l = 1$ and consequently, as they noted, to second-order ($m = 2$) analogues only. In (4) the α_n and β_n are expressed as local constants that nevertheless evolve with time globally, or as global functions $\alpha_n(O, I)$ and $\beta_n(O, I)$ of the input $I(t)$ and the output $O(t)$, thus accounting for nonlinearity in the input-output relationship globally rather than locally. We demonstrate here that these global functions, which we call "closure" expressions, can be deduced from a "training" interval of solar wind VB_s and Dst index data, and that (4), with these predetermined closure expressions included, can then be integrated using input VB_s to predict output Dst that are outside the training interval. Thus we demonstrate that (4) is a potential Dst index predictor which also allows for a study of the local timescales, coupling strength, dissipation rates, etc., contained in the input to output data coupling.

Although, in principle, the transformation from the filter relation (3) to the analogue (4) can now be carried out for any order of m and l, with the exception of $m = 1$ (see KEA), we will only present two examples: $m = 2$ with $l = 4$, and $m = 3$ with $l = 2$. In these examples we use solar wind VB_s and Dst index data for input and output respectively. For the $m = 2$ case we have studied the sequence $l = 1 \rightarrow 4$ to examine the consequences of applying such high-order derivatives to the VB_s time series as are implied by (4). We have found that the β_n converge to zero rapidly with increasing n and the results that are obtained actually improve, but only slightly, as l is increased.

The transformations of filter relation (3) to analogue (4) often produce complex analogues. In this case, even if the input $I(t)$ is real, the output $O(t)$ is complex. KEA noted this property but postponed a study of its consequences. We find that third-order analogues ($m = 3$) produce real output while second-order analogues ($m = 2$) produce complex output. It should be noted that all of these analogues contain hidden variables. A real second-order analogue for Dst is equivalent to a pair of first-order ordinary differential (ODE) equations, one for Dst and another for a hidden, and undefined, dependent variable. From this perspective, a complex second-order analogue is equivalent to a fourth-order ODE system with three hidden variables. Below, using solar wind VB_s for input, we show that the real part of the complex output of the second-order analogues gives a good representation of the Dst index data.

For their study, KEA used 1-hour time resolution data that had been interpolated to 15-min resolution. We have examined the role of the time step size by interpolating the data used by KEA even further. We have found that for the solar wind VB_s input to Dst index output coupling problem, it is essential that the time steps are at 15 min or, better, less. In view of the artificial nature of those interpolated data, we have applied the method of KEA to approximately 6 months of high time resolution (5 min) data in order to ensure that the success of the method is unrelated to interpolation or smoothing. The results of this high time resolution study of the magnetospheric coupling of solar wind VB_s input to Dst index output are presented below.

In the next section we outline the method of KEA plus our extensions and corrections to it. We show that the method proceeds in two steps. At the conclusion of the first step local-linear analogues are obtained which allow for an examination of the time local relationship between storm activity and phase and solar wind input. A detailed examination of the dynamics involved in a single storm is given. In the same section, the second step in the method of KEA is taken to obtain nonlinear analogues that can be used for prediction. The remaining sections of this paper are then directed toward an evaluation of these nonlinear analogues for Dst index prediction.

The data which we have examined using the local-linear analogues are used again as a training interval. Three nonlinear analogues are constructed using the training data to fix the free parameters in the analogues. These analogues are then tested by comparing their predictions to measured Dst data outside the training interval. Generally, we find that the analogues are successful Dst index predictors when there are no significant solar wind dynamic pressure increases.

Finally, a comparison of the analogue performance to that of the Burton et al. model is given. We give two comparisons. In the first the Burton et al. model contains parameters derived empirically from the data under consideration in this study. In the second we use the model parameters derived empirically from much earlier data by *Burton et al.* [1975]. We present this comparison with the important proviso that the Dst index data that we use in this study are not pressure corrected. However, we do present simultaneous solar wind dynamic pressure data with these comparisons so that intervals that are affected by variable or strong pressure can be discerned.

2. Method

The method for constructing data-derived analogues is described in detail in KEA except for the generalization to $l > 1$ introduced here. This generalization is implemented simply by fitting polynomials of order $l-1$ to the $I(t-n\Delta t)$ in (3) and then using the polynomials to construct expressions for the derivatives of the input data. From (3) it can be seen that there are l independent B_n filter coefficients which couple the past input $I(t-n\Delta t)$ to the predicted output $O(t+\Delta t)$. The polynomial of order $l-1$ also contains l independent coefficients, and l derivatives. Thus this procedure produces a unique map of the l input terms on the right side of (3) to the l derivatives on the right side of (4), thereby removing the mismatch in the number of degrees of freedom contained in the map as presented by KEA. A further discussion of this generalization, with an example calculation, is given in Appendix A.

In addition, we have, as noted above, extended the method to encompass complex analogues. No other modifications have been made.

We wish to emphasize here that two steps are necessary to construct the data-derived analogues:

2.1. Step 1: Local-Linear Analogue

2.1.1. Construction. The local-linear filter coefficients in (3) are computed from the input-output data as described in *Vassiliadis et al.* [1995] except for two points: (1) Instead of nearest neighbors (which are near each other in phase space), time local neighbors (near in time) are used. The time local neighbors are obtained from a window in time surrounding the present time t. These neighbors form a matrix, the delay matrix, which is inverted to yield the local-linear filter coefficients (see *Vassiliadis et al.* [1995]). (2) Just prior to its inversion, the delay matrix is decomposed into a singular-value basis [*Press et al.*, 1992; *Golub and Van Loan*, 1996] and the contributions of all of the singular values except the largest one are set to zero. This step, in effect, produces an expansion of the local-linear filter coefficients in terms of an empirical eigenbasis; the expansion is then truncated to a single term by the neglect of the smaller singular values (empirical eigenvalues). KEA found that this truncation is necessary to obtain the local-linear filter coefficients for the highest-frequency component of the input-output data, but it is this truncation that also leads to complex analogues. We are actively studying the implications of this key step and will report our findings at a later time.

Having obtained the local-linear filter coefficients in this manner, (3) is Fourier transformed. Since, for nonlinear coupling, (3) is only locally valid, it is necessary to imagine a proxy $O(t)$ which coincides with the real output data at the time steps involved in (3) but otherwise is generated by (3) both forward and backward in time using the locally valid filter coefficients A_n and B_n; the measured input data $I(t)$ is used for this purpose. Using the notation $\mathcal{F}O(t) = \overline{O}(\omega)$, then $\mathcal{F}O(t-n\Delta t) = q^{-n}\overline{O}(\omega)$ in which $q = \exp(i\omega\Delta t)$, Δt is the data time interval, and ω is the Fourier variable. In this manner, the transfer function relation

$$\overline{O}(\omega) = \overline{I}(\omega)\left[\frac{\sum_{n=0}^{l-1} B_n q^{m-1-n}}{q^m - \sum_{n=0}^{m-1} A_n q^{m-1-n}}\right] \tag{5}$$

is obtained. In the denominator of this expression the A_n filter coefficients determine the positions of the zeros in the mth order polynomial in q, and thus the positions of poles on the complex q plane, and finally the positions of singularities on the complex ω plane.

Treating (4) as locally linear, its solution can be written explicitly. For example, if $m = 2$ and $l = 1$, then

$$O(t) = c_1 \exp(i\omega_1 t) + c_2 \exp(i\omega_2 t) + S(t) \tag{6}$$

in which

$$S(t) = \beta_0 \int_0^t ds\, K(s) I(t-s) \tag{7}$$

$$K(s) = \frac{e^{i\omega_1 s} - e^{i\omega_2 s}}{i(\omega_1 - \omega_2)} \tag{8}$$

Notice that the solution is completely determined by the two frequencies ω_1 and ω_2.

KEA produced a map of the A_n and B_n in (3) to the α_n and β_n in (4) which ensures that the continuous solution (6), when evaluated at the discrete data times in (3), agrees with the data values in (3). This was accomplished by ensuring that the frequencies $\omega_1, \omega_2, \ldots \omega_m$ are at the positions of the singularities in the transfer relation (5), and by fixing the values of the β_n ($n = 0$ only in KEA; here we extend their method to arbitrary n). using the appropriate kernel $K(s)$ to relate them to the B_n.

At the end of this first step, a "local-linear analogue" is achieved. This is an analogue of the form (4) in which a set of $\alpha_n(t)$ and $\beta_n(t)$ exists at each time step. The number of coefficients in (4) at the end of this step is identical to the number of filter coefficients in (3), $l+m$ for each time step. This local-linear analogue has the sole purpose of providing an interpretation of the local-linear filter coefficients in terms of the well-known effects of coefficients in low-order ODE's; i.e., timescales, dissipation rates,

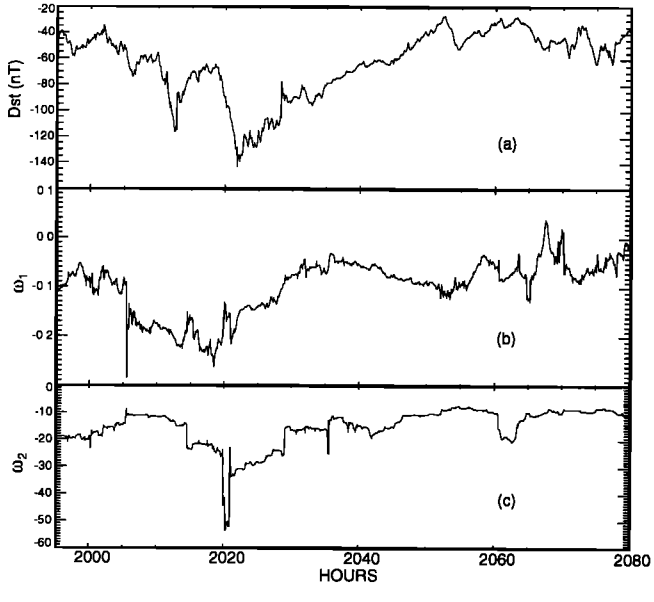

Figure 1. (a) Measured *Dst*, (b) decay rate obtained from a local-linear analysis, (c) growth rate obtained from the same analysis. The abscissa is time since the beginning of the data set.

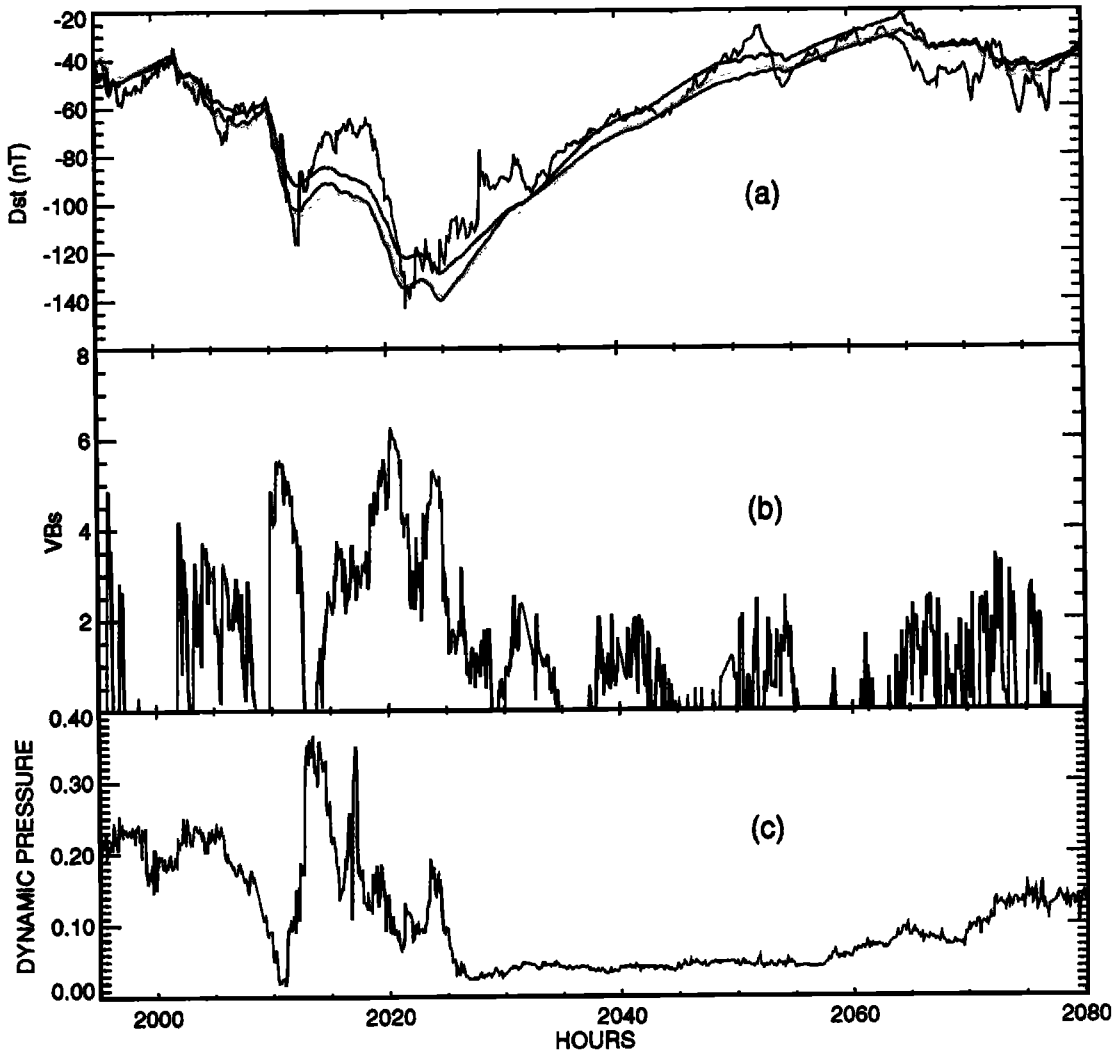

Plate 1. Training interval for three analogues. (a) Measured Dst (black) and analogue outputs (red and green, see text). (b) Solar wind VB_s (mV/m) used to both train and drive the analogues. (c) Solar wind dynamic pressure. The abscissa is time since the beginning of the data set.

coupling strengths, etc. Before proceeding to the second step in this construction we provide an example of this type of analysis.

2.1.2. Application: A local-linear storm analysis. Figure 1 shows a small portion of the Dst index data used for this study. Simultaneous solar wind VB_s and dynamic pressure are shown in Plate 1. The solar wind data were obtained on the ISEE 3 spacecraft at L1; they have been propagated ballistically to an average magnetopause position using the time-dependent solar wind velocity at ISEE 3. The Dst index data have not been corrected for variations in solar wind pressure. Although Dst is usually an hourly index, in this case the data are at 5-min resolution, and they span the first 6 months of 1979. There are 1065 data points shown in Figure 1.

A local-linear analogue of the form (4) with $m = 2$ and $l = 1$ has been constructed using the method due to KEA as outlined above. In contrast to the approach that will be taken in the next section below (step 2: nonlinear analogue), the expansion of the local-linear filter coefficients in terms of an empirical eigenbasis was not truncated. At each time step in the data a set $(\alpha_0, \alpha_1, \beta_0)$ was obtained using a window of width 15 hours to construct the time local neighbors. Equivalently, at each time step in the data a pair of frequencies ω_1 and ω_2 and the coupling coefficient β_0 were obtained. For the Dst index and VB_s data in this interval, both frequencies were found real and negative; they are plotted in the second and third panels of Figure 1. As shown by KEA, when these frequencies are both real and negative, and if their values are disparate, then the impulse response of this second order analogue is close to that of the first-order *Burton et al.* [1975] model of the VB_s to Dst coupling; the second-order system mimics (locally) that of their first-order model. This is the case for the data shown in Figure 1 and Plate 1. The analogue responds to an impulse rapidly at first over a timescale which is the inverse of the absolute value of ω_2 shown in the third panel of Figure 1, and then it relaxes slowly over a timescale which is the inverse of the absolute value of the decay rate ω_1 shown in the second panel. These two phases correspond to the main and recovery phases of an idealized storm which is the result of an impulse in VB_s. Within the context of the Burton et al. model, the evolution of the decay rate during the recovery phase of observed storms has been studied extensively (see review by *Feldstein* [1992] and references therein). This evolution is direct evidence for the nonlinearity of the VB_s to Dst coupling; if the coupling were linear as the Burton

et al. model assumes, then the decay rate would be constant. The second and third panels of Figure 1 show the detailed evolution of ω_1 and ω_2 obtained using the method due to KEA.

For the following discussion the absolute values of the rates shown in Figure 1 will be assumed. Then the rates can be expressed as inverse timescales. From the third panel of Figure 1 it can be seen that the timescale associated with ω_2 is always very small, ranging from at most 10 minutes down to as little as 1 min; initial responses to the VB_s input are unexpectedly fast. This result is due to a combination of two factors: (1) The VB_s and *Dst* data are at higher time resolution than normal, and (2) the precise local-linear analysis is capable of revealing these short timescales in the data. The second panel of Figure 1 indicates the rate at which *Dst* would recover following its response to an impulsive VB_s input and assuming that the VB_s input is zero during the recovery. At the beginning of the interval shown in Figure 1 the decay rate is $\approx$ 1/10 hours^{-1}. The main phase of the storm proceeds in stages because the VB_s input is not steady. During the main phase the decay rate increases until just before the minimum in *Dst* when it reaches a value $\approx$ 1/4.3 hours^{-1}. Notice that the very rapid decrease in *Dst* leading to its minimum at time $\approx$ 2022 hours is reflected in a significant increase in ω_2 shown in the third panel of Figure 1 at time $\approx$ 2020 hours. The decay rate starts to decrease before the minimum in *Dst* during the rapid decrease of *Dst*. It is doubtful, however, that the decay rate plays any role in the evolution of *Dst* at this time; the evolution is certainly controlled by the exceptionally large ω_2 just before the *Dst* minimum. Following the minimum, as the recovery phase progresses, the decay rate decreases as expected [*Feldstein*, 1992] until it reaches a value $\approx$ 1/20 hours^{-1} at time $\approx$ 2035 hours. It can be seen from the first panel of Figure 1 that the recovery of this storm does not slow as it progresses and, consequently, the decay rate actually increases in the final stage of the recovery. There is nothing in the simultaneous VB_s and dynamic pressure data shown in Plate 1 to explain this unusual behavior. If anything, it might be thought that the weak VB_s pulses at times $\approx$ 2040 and 2050 hours would help to slow or even reverse this recovery. However, these pulses appear to produce no effect, a fact that will be explored further in the next paragraph. Following the recovery, the evolution of both the *Dst* index and the decay rate is erratic; we have been unable to discern any systematic behavior following time $\approx$ 2055 hours.

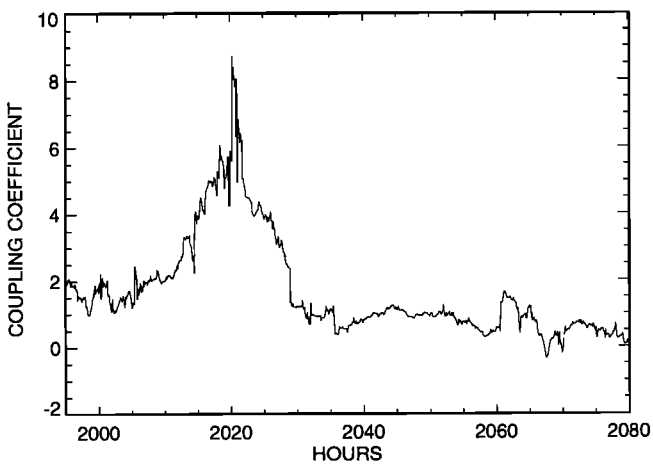

Figure 2. The evolution of the local-linear coupling parameter β_0. The abscissa is time since the beginning of the data set.

Figure 2 shows the evolution of the coupling parameter β_0 during the time interval discussed in the preceding paragraph. This is the parameter that multiplies VB_s on the right side of (4); the driver of the *Dst* response is the product $\beta_0 \times VB_s$. The coupling parameter peaks strongly during the rapid *Dst* descent at time $\approx$ 2020 hours. Generally, the coupling is strongest during the peak of the storm. The weak coupling before this storm has not been seen before, but the even weaker coupling during the storm recovery has been reported earlier by KEA as typical. Apparently, the driver of storm activity is not just simply the solar wind VB_s parameter; the relationship to VB_s is more complicated than a simple linear one. During this interval the solar wind dynamic pressure is variable but generally weak, particularly during the recovery phase of the storm. Further, KEA found this behavior for essentially all recoveries; it appears the complicating factor is not the dynamic pressure. Finally, we note here that the failure of the weak VB_s pulses at times $\approx$ 2040 and 2050 hours to help slow or even reverse the recovery can be understood on the basis of the weak coupling to VB_s during the recovery phase.

2.2. Step 2: Nonlinear Analogue

The local-linear analogue cannot be used for prediction since it requires input and output data both from the past and the future to compute a set of $\alpha_n(t)$ and $\beta_n(t)$. To construct a predictive tool, a second step is necessary.

On studying the evolution of the $\alpha_n(t)$ and $\beta_n(t)$ in the local-linear analogue, KEA found that these coefficients could be well approximated by simple functions of the VB_s and *Dst* data. They found $\alpha_n(t) \approx \alpha_{n0} + \alpha_{n1}(d \ln Dst/dt)$ and $\beta_n(t) \approx \beta_{n0} + \beta_{n1}(VB_s/Dst)$ when $Dst < 0$. The free parameters α_{ni} and β_{ni} $(i = 0, 1)$ were found reasonably independent of the particular data interval used for their construction. Thus they introduced the "closure relations"

$$\alpha_n(O) = \alpha_{n0} + \alpha_{n1}\left(\frac{d \ln O}{dt}\right)$$
$$\beta_n(O, I) = \beta_{n0} + \beta_{n1}\left(\frac{I}{O}\right) \tag{9}$$

to replace the $\alpha_n(t)$ and $\beta_n(t)$ in (4). In these relations, the O stands for the dependent output variable in the m'th order ODE, not the output data, while the I still stands for the input data; nonlinear analogues result. Generally, a large reduction in the number of free parameters is accomplished. For example, if an interval of one thousand data points were used to find the local-linear coefficients, then the one thousand values of $\alpha_1(t)$ would be replaced by the two parameters α_{10} and α_{11}. Further, having fixed the α_{ni} and β_{ni} $(i = 0, 1)$ to obtain good in-sample predictions of $O(t)$ in a "training interval," then these values can be retained and the nonlinear form of (4) integrated using out-of-sample $I(t)$ to predict out-of-sample $O(t)$. This construction and application are demonstrated below.

3. In-Sample Training

The black curve in the first panel of Plate 1 repeats the *Dst* index data discussed in the previous section and the subsequent panels show the simultaneous solar wind VB_s parameter and dynamic pressure. The data shown in Plate 1 have been used to fix the α_{ni} and β_{ni} in the closure relations (9) for three analogues; we call this process "training." The first of these analogues is third-

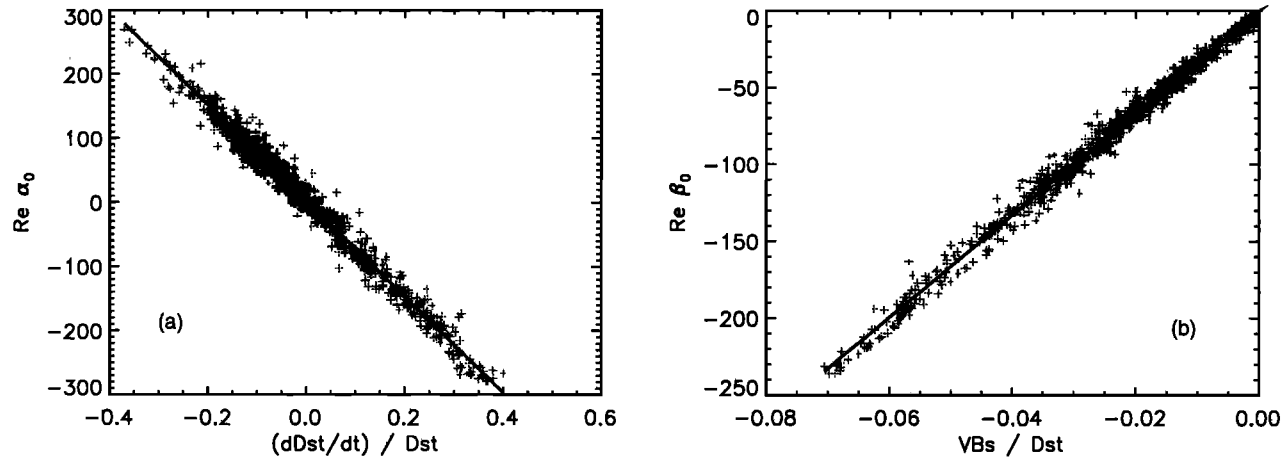

Figure 3. Samples of linear fits to the distributions of local-linear coefficients $\alpha_n(t)$ and $\beta_n(t)$ obtained for the third-order analogue ($m = 3$, $l = 2$) from the data shown in the training interval of Plate 1.

order with a two-term driver ($m = 3, l = 2$), and the other two are second-order with four-term drivers. For each of these analogues, the "step 1" procedure outlined above was carried out to obtain the 1065 sets of local-linear coefficients $\alpha_n(t)$ and $\beta_n(t)$ (a complete set for each of the 1065 data points). Then "step 2" was carried out to construct the closure relations; Figure 3 illustrates the basis of this construction using samples of the $m = 3$ calculation.

The crosses in Figure 3a show the 1065 values of $\alpha_0(t)$, obtained from the training interval of Plate 1, plotted against the corresponding values of $d(\ln Dst)/dt$. The crosses in Figure 3b show the 1065 values of $\beta_0(t)$ plotted against the corresponding values of VB_s/Dst in that interval. These are samples of the third order calculation ($m = 3$) which leads to a real analogue; the coefficients are real. Also shown in these figures are linear fits to the distributions of $\alpha_0(t)$ and $\beta_0(t)$. Each of these fits replaces the 1065 values of the respective coefficient with two numbers, the intercept and the slope of the fit. The transition from the local-linear form of (4) to the nonlinear form of (4) is effected by substituting the closure relations (9) into (4) with the α_{ni} and β_{ni} ($i = 0, 1$) given by the intercepts and slopes of these fits. The third-order analogue ($m = 3$, $l = 2$) contains ten such intercepts and slopes which are held fixed throughout the training interval, and in any application of the analogue outside the training interval. A complete set of intercepts and slopes (ten numbers in this case) constitutes a single nonlinear analogue. Such an analogue can be integrated, using input VB_s data from any source, to produce predicted Dst. In general, each analogue contains $2(m + l)$ intercepts and slopes (they each may be complex) which are fixed by linear fits to the local-linear coefficients as shown in Figure 3.

The red curve in the first panel of Plate 1 shows the result of integrating the third-order analogue using the VB_s data shown in the second panel for input. This is an in-sample integration; the input VB_s data and the Dst index data to which the analogue output is compared are the same data from which the analogue was constructed. The green curves show the real parts of the outputs obtained from two complex second-order analogues ($m = 2$, $l = 4$) that were also constructed from the data in this training interval. Using this high time resolution data, we have found it necessary to smooth the data somewhat to produce reliable closure relations. The two second-order analogues differ in the amount of smoothing that was applied. Moving box car averaging was done with a 25 min window in one case and a 35 min window in the other. None of the data shown in Plate 1, however, have been smoothed, and the analogue outputs shown there were obtained using unsmoothed VB_s data for input; the smoothing was applied only in the training process. All of these analogues will be applied to out-of-sample data below; the same color conventions will be in effect.

The third panel of Plate 1 shows the solar wind dynamic pressure during the training interval. In other intervals, which will be discussed below, the dynamic pressure occasionally takes on large enough values to significantly affect the nonpressure-corrected Dst. It appears that this is not the case in this training interval, a fact that was instrumental in choosing this interval to train the analogues. By construction, the analogues respond to the solar wind solely through the VB_s parameter. The training interval was chosen to ensure that the solar wind VB_s was, indeed, the dominant driver of the measured Dst.

The correlations between analogue outputs and measured Dst are in the range 0.94–0.96 in this training interval, and the rms errors are in the range 10–12 nT. Clearly, the real parts of the complex second-order analogue outputs do approximate the measured Dst.

4. Out-of-Sample Predictions

The VB_s data shown in Plate 2 have been used as input to the three analogues extracted from the training interval data to produce the out-of-sample comparison of modeled and measured Dst shown in the top panel. In this case the cross correlations between analogue outputs and measured Dst are in the range 0.67–0.70, and the rms errors are in the range 22–26 nT. A representative sample of successes and failures are shown. All three analogues yield good estimates of the storm peak times in the complex activity at $\approx$ 1200 hours but they also overestimate the peak values considerably. Conversely, the analogues give an excellent representation of the storm at $\approx$ 1600 hours.

Before and after the storm at 1600 hours in Plate 2, the analogues respond to significant signals in the VB_s input but the measured Dst does not. These intervals have the appearance of being influenced by the solar wind dynamic pressure increases shown in the third panel, a response which is not included in the analogues. In the same vein, the measured Dst peak values in the complex activity at $\approx$ 1200 hours have probably been pushed

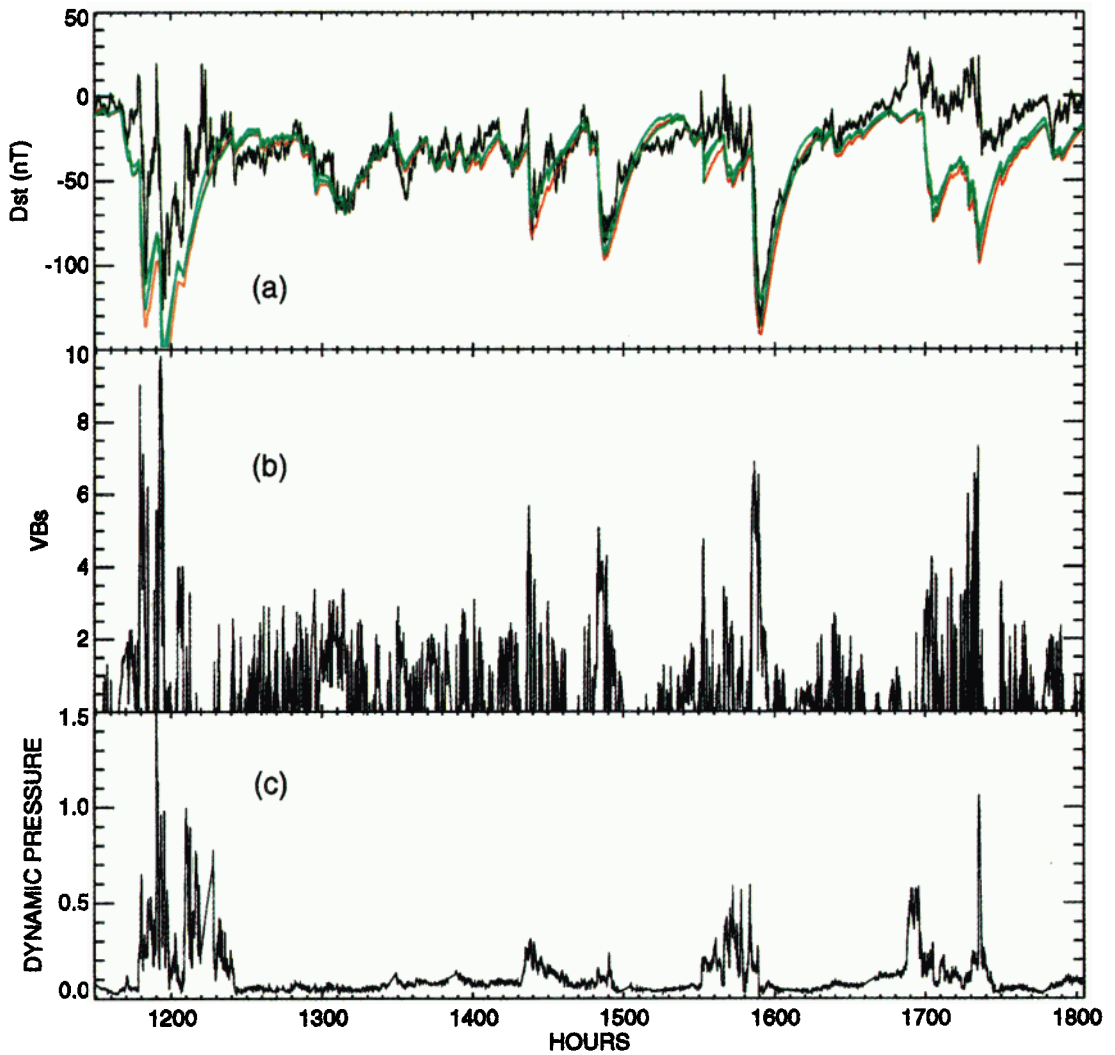

Plate 2. Testing interval for three analogues. (a) Measured Dst (black) and analogue outputs (red and green, see text). (b) Solar wind VB_s (mV/m) used to drive the analogues. (c) Solar wind dynamic pressure. The abscissa is time since the beginning of the data set.

up by the large dynamic pressure during that interval. Again, since the analogues cannot respond to the dynamic pressure, they overestimate the magnitude of the peak values. Thus all of the significant differences between the measured and predicted Dst in this interval can be explained by the lack of response to the solar wind dynamic pressure in the analogues. Otherwise, the analogues give a good representation of the measured Dst over a long interval of data when the solar wind dynamic pressure is low and roughly constant.

A second out-of-sample application of the three analogues is shown in Plate 3. In this case the cross correlations between analogue outputs and measured Dst are in the range 0.76–0.80, and the rms errors are in the range 22–26 nT. The poor performance at $\approx$ 2000 hours is an artifact. Interpolation through a VB_s data gap has produced a prolonged input pulse that probably did not occur but to which the analogues all respond.

With the exception of the poor performance at $\approx$ 2000 hours, the analogues give a good representation of the measured Dst until after the large storm at $\approx$ 2150 hours when it appears that increased solar wind pressure is again playing a large role. In this case a definite statement cannot be made because of a data gap containing the interval in which the pressure appears to have increased. Another characteristic behavior of these analogues appears near the end of this interval. From $\approx$ 2300 to 2400 hours the VB_s data contain a series of low amplitude, short-duration impulses. The result is that the measured Dst hovers near zero, while the analogue outputs remain steadily below. This behavior will be discussed further in the next section.

A comparison shows that the training interval of Plate 1 is contained in the interval shown in Plate 3. Of the two large storms shown in Plate 3, the relatively smaller one is the one that was used for training. The performance of the analogues in predicting the larger storm illustrates an important advantage that they have. It was not necessary for the analogues to have experienced such a large storm in their training in order to predict its occurrence reasonably well.

5. Comparison With *Burton et al.* [1975] Model Performance

The model due to *Burton et al.* [1975] responds to the solar wind through the VB_s parameter and predicts the pressure-

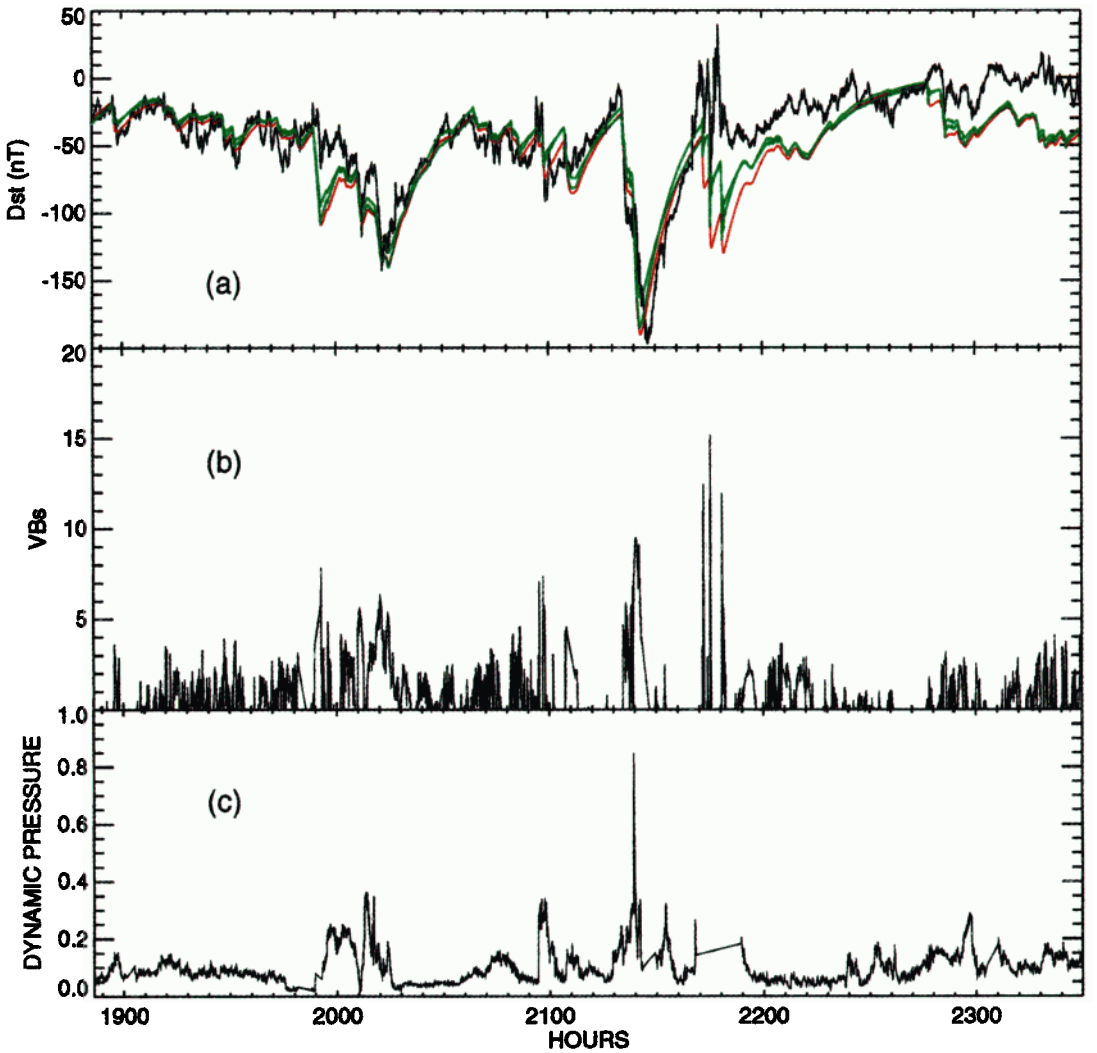

Plate 3. Testing interval for three analogues. (a) Measured Dst (black) and analogue outputs (red and green, see text). (b) Solar wind VB_s (mV/m) used to drive the analogues. (c) Solar wind dynamic pressure. Abscissa is time since the beginning of the data set.

corrected Dst_0 in which the contribution of the disturbed ring current has been maximized. The model is given by (1) in which τ and β are constants. Thus the Burton et al. model is first-order and linear. To integrate this equation numerically it can be discretized in a variety of ways, the simplest of which is given by

$$Dst_0(t + \Delta t) = \left(1 - \frac{\Delta t}{\tau}\right) Dst_0(t) + \Delta t\, \beta\, VB_s(t) \quad (10)$$

in which we have replaced $F(E)$ by VB_s. If Δt is chosen equal to the time step in discrete data, then (10) is a simple linear ARMA filter relation of the form (3). Thus numerical integration of (1) amounts to iteration of the filter relation (10) using, in both cases, the measured VB_s as input and the measured $Dst_0(t = t_0)$ for an initial condition.

For pressure-corrected Dst_0 as output and solar wind VB_s as input, and with $m = 1$ and $l = 1$, (3) reduces to

$$Dst_0(t + \Delta t) = A_0\, Dst_0(t) + B_0\, VB_s(t) \quad (11)$$

Generally, the relationship between VB_s and Dst_0 is nonlinear and, consequently, the filter coefficients A_0 and B_0 evolve with time. However, if the window that is used to find time local neighbors is made large, so large that the relationship between VB_s and Dst_0, averaged over the window, becomes stationary, then a linear approximation to (11) is obtained in which the filter coefficients A_0 and B_0 do not evolve with time [*Vassiliadis et al.*, 1995; *Klimas et al.*, 1997]. In this limit the local-linear filter relation (11) becomes globally linear and identical to (10) with $A_0 = (1 - \Delta t/\tau)$ and $B_0 = \Delta t\beta$. Thus, in the linear limit the data derived filter coefficients can be used to fix the values of the parameters τ and β in the Burton et al. model. We have carried this out using a window of width 2500 hours, or 30001 data points at 5-min resolution. From the filter coefficients in this linear limit, we find $\tau \approx 16$ hours and $\beta \approx 2.76$ $((\text{mV/m})\text{hr})^{-1}$. In the following we iterate the linear filter relation to, in effect, integrate the Burton et al. model, and we compare the performance of this discretized Burton et al. model with that of the nonlinear analogues discussed in the previous section. We show the comparison in the three data intervals discussed in the preceding section, in the training interval shown in Plate 1 and in the two testing intervals shown in Plates 2 and 3. It should be noted that the Dst data under consideration here has not been

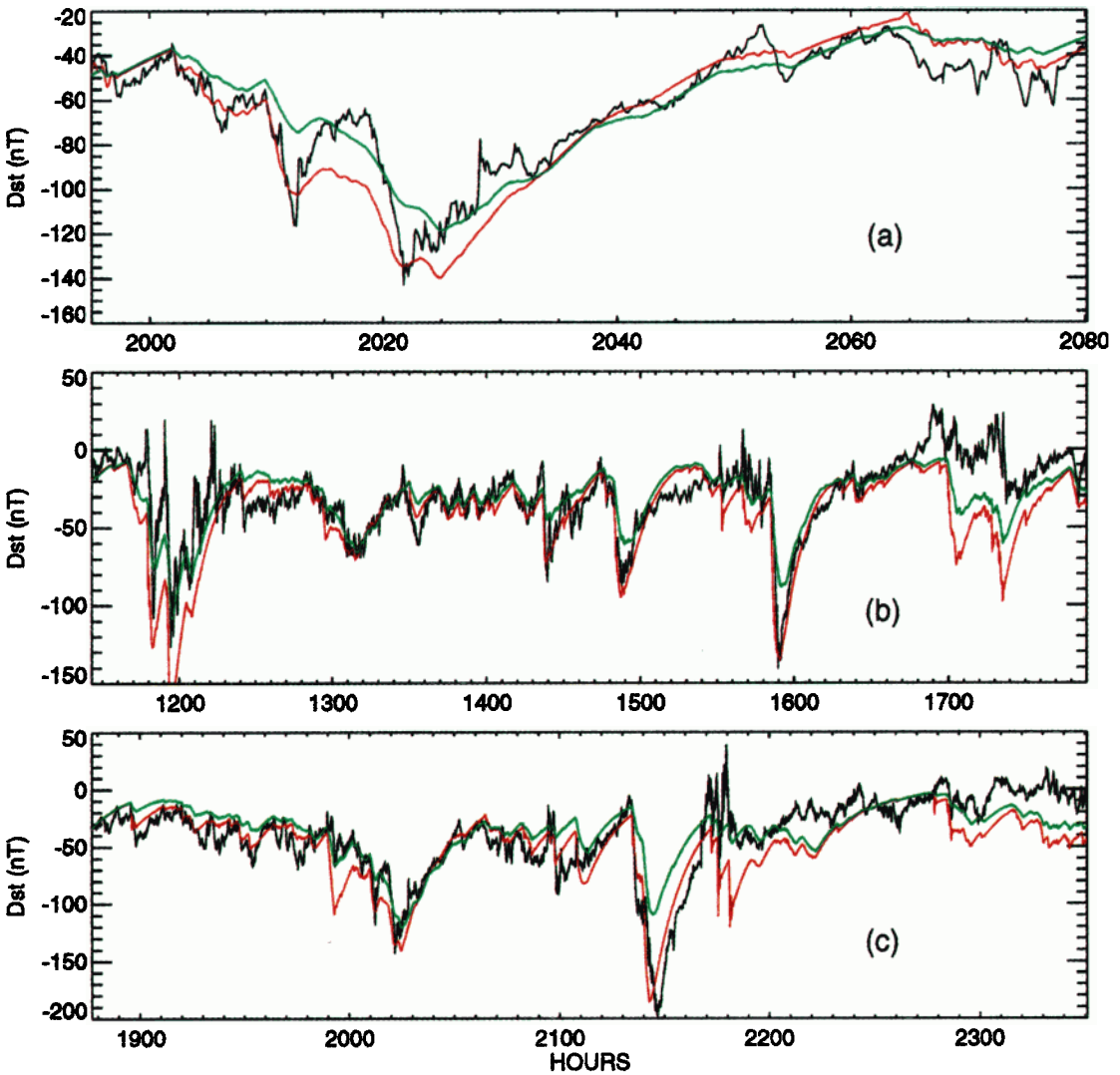

Plate 4. Comparison of measured Dst (black), analogue ($m = 2$, $l = 4$) output (red), and discretized *Burton et al.* [1975] model output (green) over (a) the training interval shown in Plate 1, (b) the testing interval of Plate 2, and (c) the testing interval of Plate 3.

pressure-corrected, and thus both the Burton et al. model and the nonlinear analogues should not be expected to perform well during the significant dynamic pressure increases discussed in the preceding section.

In Plate 4 the Burton et al. model and nonlinear analogue outputs are compared to each other and to the measured Dst in the training and two testing intervals. Some standard measures of performance favor the Burton et al. model somewhat. When compared to the measured Dst, the rms error is 11.4 nT for the nonlinear analogue and 10.4 nT for the Burton et al. model in the training interval, it is 23.4 nT for the analogue compared to 16.1 nT for the linear model in the first testing interval, and it is 22.3 nT for the analogue versus 21.9 nT for the linear model in the second testing interval. If the portions of the first testing interval containing pressure pulses are removed from these computations, then the rms errors decrease to 13.7 nT for the nonlinear analogue and to 12.1 nT for the Burton et al. model. The cross correlations between modeled and measured Dst are mixed. The cross correlation is 0.96 for the nonlinear analogue and 0.92 for the Burton et al. model in the training interval, it is 0.68 for the analogue compared to 0.73 for the linear model in the first testing interval, and it is 0.80 for the analogue compared to 0.77 for the linear model in the second testing interval. The nonlinear analogue tends to overpredict the amplitude of the Dst disturbance between Dst peaks. A good example of this kind of behavior can be seen in the first panel of Plate 4 just before and after the storm peak at time $\approx$ 2022 hours. During these times the Burton et al. model performance is better. On the other hand, the Burton et al. model tends to underpredict the Dst disturbance amplitude at the times of the peak disturbances while the nonlinear analogue does quite well at these times. Examples are the storm peak in the training interval, the peaks at times $\approx$ 1440, 1490, and 1590 hours in the first testing interval, and the major storm at time $\approx$ 2150 hours in the second testing interval. It is interesting that the Burton et al. model also overpredicts at the end of the second testing interval, from time $\approx$ 2300 hours onward when the VB_s input consists of a series of low amplitude, short duration pulses. *Gonzalez and Tsurutani* [1987] have pointed out that VB_s input of this character does not produce a significant response in Dst but both the Burton et al. model and all of the analogues

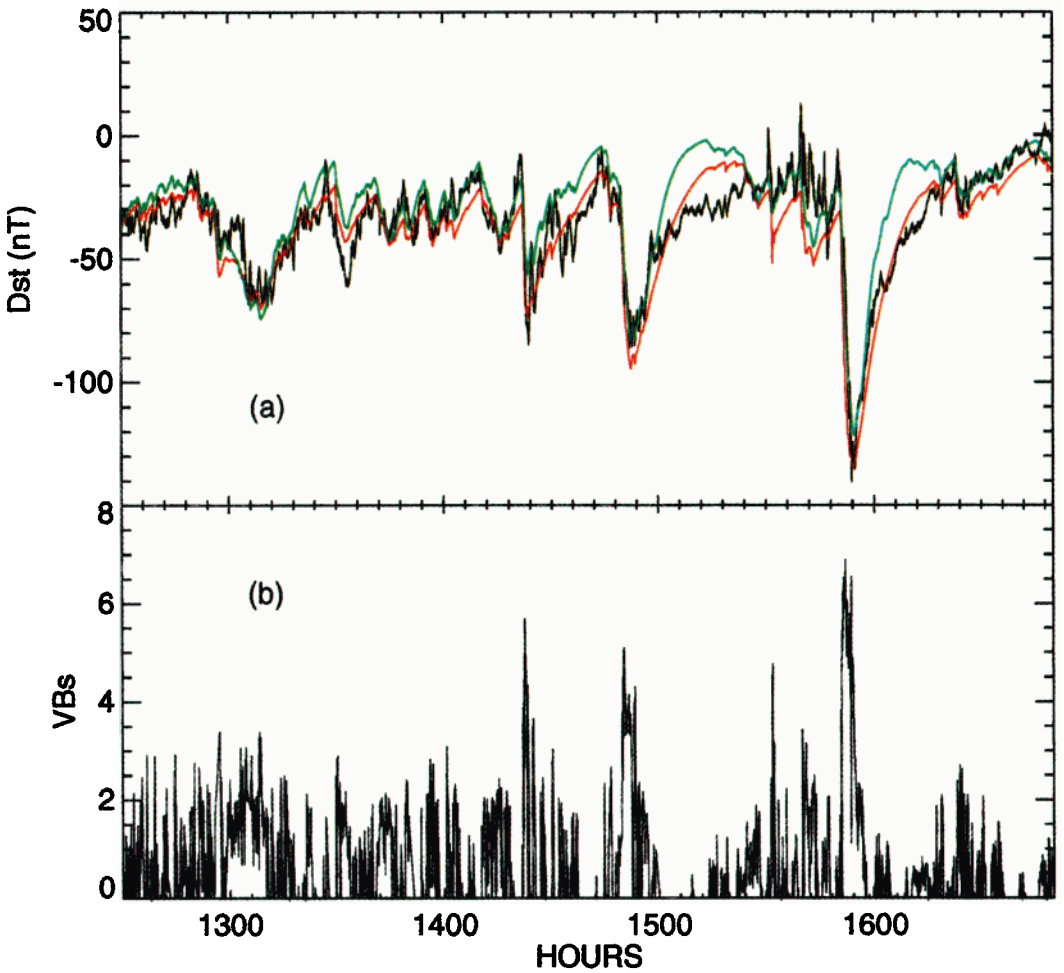

Plate 5. Performance comparison of nonlinear analogue ($m = 2$, $l = 4$) with second discretized *Burton et al.*[1975] model. (a) Measured Dst (black), analogue output (red), and model output (green). (b) Simultaneous solar wind VB_s parameter.

do respond. *Burton et al.* [1975] found it necessary to filter high frequencies out of the VB_s input. Following their lead, we have smoothed the VB_s data and found that the performance of the analogues is improved during this interval, and also particularly during the interval before time $\approx$ 2200 in which the analogues have a strong response to the narrow spikes in VB_s. However, the amount of smoothing that we have had to apply in order to achieve a significant improvement is considerable; we smoothed with a running box car average of width 100 min. We do not consider this an acceptable approach to improving the performance of the analogues and must conclude at this time that this behavior in both the linear model and the analogues remains unexplained. Notice that the Burton et al. model does quite well during the pressure pulses in the first testing interval, during the major storm at time $\approx$ 1200 hours and just before the storm at time $\approx$ 1590 hours. This performance is probably accidental however, the tendency of both analogue and linear model to overpredict during pressure pulses being balanced by the overall tendency of the linear model to underpredict peak disturbance values.

In the preceding comparison we have used the values for τ and β in the Burton et al. model that we have extracted from the data under consideration in this study. These values are not in agreement with those obtained by *Burton et al.* [1975] in their study of a different data set ($\tau = 7.7$ hours and $\beta = 5.4$ $((\text{mV/m})\text{hr})^{-1}$). We have carried out the comparison discussed in the preceding paragraph using a second version of the Burton et al. model in which their parameter values were used rather than ours. Some representative details of the comparison are shown in Plate 5. In contrast with the first version, this second version of the Burton et al. model does more poorly than the nonlinear analogue when performance is measured by rms error and cross correlation. Over the interval shown in Plate 5 the rms error of the nonlinear analogue is 10.4 nT while that of the Burton et al. model is 13.0 nT. The cross correlation of the analogue output with measured Dst is 0.89 while that of the Burton et al. model is 0.84. This version of the Burton et al. model does much better in predicting the storm maxima than the first version however. While the nonlinear analogue continues to do better with the storm maxima, the difference is small. Interestingly, the Burton et al. model usually predicts the initial storm recovery rate quite well but it fails to predict the later slowing of the recovery. This behavior is evident for the two storms in Plate 5 at times $\approx$ 1490 and 1590 hours. Since the Burton et al. model contains only one constant relaxation timescale, this behavior might be expected. The second-order nonlinear analogue also contains only one relaxation timescale but it varies with time and, consequently, the analogue generally does better in this respect.

Both versions of the *Burton et al.* [1975] model and the non-

linear analogue perform roughly equivalently. The first version of the Burton et al. model, which was derived empirically from the present data, does better than the nonlinear analogue overall. However, that version does poorly in predicting storm maxima when compared to the analogue. The second version of the Burton et al. model, which was derived empirically from much earlier data by *Burton et al.* [1975], does more poorly than the nonlinear analogue overall with the present data, but it does much better with storm maxima than the first version. Thus, in an application in which the overall performance and the storm peak values are important the nonlinear analogue would be preferable.

6. Summary

The method due to KEA for constructing data-derived input-output analogues has been generalized. Higher-order analogues with higher-order driver expressions have been constructed and studied. In all cases it has been found that the closure relations (9) remain satisfied. Complex analogues have been constructed and studied. It has been shown that the real part of the complex output of these analogues approximates the Dst index data. The training and testing discussed above was carried out using high time resolution data, thus demonstrating that the results of KEA were not due to the interpolated nature of the data that they used.

The construction of KEA proceeds in two steps. At the conclusion of the first step empirical local-linear analogues are obtained which allow for an examination of the dynamical properties of the input-output physical system under consideration. A detailed study of the dynamics involved in a single storm has been presented. The relationship between VB_s input and Dst output for this storm can be described in the context of the Burton et al. model, but with variable decay time and coupling strength; the evolution of these parameters over the course of the storm has been discussed. A more comprehensive local-linear analysis of these data is in progress and will be reported at a later time. We have emphasized that the local-linear analogues cannot be used for prediction applications.

For the second step of the KEA construction, empirical closure relations are found. These allow for the replacement of the parameters of the local-linear analogues by functions of the input data and output variable; nonlinear analogues result. In this manner, the storm interval which has been subjected to a local-linear analysis, as discussed in the preceding paragraph, has also been used to construct three empirical nonlinear analogues. These have then been tested for their ability to predict Dst index data out of sample; i.e., outside of the storm interval used for the construction. The prediction performance of one of these analogues has been compared to those of two versions of the Burton et al. model. In the first version the empirical model parameters were fixed using the VB_s and Dst data under consideration in this study. In the second, the empirical model parameters given by *Burton et al.* [1975] were used. The overall prediction performance of the nonlinear analogue was shown to be somewhat better; the differences are not large.

The performance of three analogues has been studied. Two of these were second order ($m = 2$) with four-term ($l = 4$) drivers and the third was third order ($m = 3$) with a two-term ($l = 2$) driver. The performance of these analogues was found approximately equivalent. Although not presented here, the transition from $l = 1$ to $l = 4$ was studied in the case of the second order analogues. As l was increased, some improvement in the performance of the analogues was obtained.

One of the second-order analogues underpredicted the variance in the Dst data in the training interval, and then continued to do so in the testing intervals. We have found this to be a common property of the analogues; those that underpredict in a training interval are found to usually underpredict in out-of-sample tests. Other characteristics that an analogue might take on in a training interval tend to persist into test intervals. Thus we imagine that it would be advantageous to integrate a group of analogues forward in time to produce a cluster of predictions at any instant with predetermined weights applied to the validity of each prediction, based on previous performance.

We have demonstrated two types of prediction failures. The first occurs during significant solar wind dynamic pressure increases, and is not surprising. The analogues have only one input, the solar wind VB_s parameter; they have no dependence on dynamic pressure. Perhaps an evolving pressure-correction, based on measured upstream solar wind dynamic pressure, can be incorporated. Multivariate treatments of the local-linear prediction model (3) have been accomplished [*Hunter and Theiler*, 1992]. Since the method of KEA is based on the local-linear prediction model, it can be expected that multivariate generalizations of this method will also be possible, thus allowing for additional solar wind parameters in the input data. It is possible that this generalization may be carried a step further to include multiple outputs, thus allowing for disturbance predictions at individual magnetometer stations as opposed to predictions of global indices.

The second type of prediction failure occurs during intervals when the VB_s input consists of a series of low amplitude, short duration pulses. During an interval of this kind, the Dst index does not respond [*Gonzalez and Tsurutani*, 1987] but the analogues do. We have found that we are able to improve the analogue performance by smoothing the VB_s input. Thus it appears that it is the short duration of the pulses that is the problem. For prediction applications, smoothing would not be an option. The solution of this problem is unknown at present, and is the subject of continuing research.

At this time the method due to KEA is new with many unexplored facets. The particular nonlinear analogues that have been presented must be considered preliminary. At present it is not known how to optimize the performance of these analogues nor have higher-order analogues, that may perform better, been studied. Nevertheless, these analogues do appear to have potential for predicting geomagnetic activity, given real-time solar wind data from L1.

In addition to producing nonlinear analogues with the potential for predicting geomagnetic activity, we have shown that the method of KEA produces a physical interpretation of the magnetospheric dynamics responsible for the coupling of solar wind driver to geomagnetic activity response. It seems likely that the operation of such physically understandable predictors will lead simultaneously to a better understanding of the magnetospheric dynamics and to improved prediction capabilities.

Appendix

KEA gave two explicit conversions of the local-linear predictor (1) to the local-linear form of the analogue (2). Their examples yielded second and third order local-linear analogues ($m = 2$ and $m = 3$) with, in both cases, one-term coupling ($l = 1$) to the input time series. As they noted, the one-term coupling is sufficient for the second order analogue, but not for the third order analogue. For $m = 3$, a minimum of two-term coupling ($l = 2$) is required

(see KEA for a further discussion). Thus their results were limited to second-order analogues. As they noted, their third- and higher-order results were inconsistent.

The inconsistency in the higher-order results of KEA has been removed through the introduction of polynomial fits to the input data in the local-linear predictor (1) plus the sum over derivatives of the input data shown on the right side of (2). In the following we reproduce the $m = 3$ calculation of KEA with these new features included. In principle, the technique shown below can be extended to any m and l. For $m = 2$ we have explicit expressions for arbitrary l; for $m = 3$ we are limited, at this time, to the $l = 2$ case shown below.

Our approach follows that of KEA closely. We treat (2) as locally linear and adjust its continuous solution so that it agrees locally with the data values that enter (1) at the discrete data times. For $m = 3$ the local solution of (2) can be written as

$$O(\tau) = c_1 e^{z\omega_1\tau} + c_2 e^{z\omega_2\tau} + c_3 e^{z\omega_3\tau} + S_3(\tau) \quad \text{(A1)}$$

in which

$$S_3(\tau) = \int_0^\tau ds\, K_3(s)\, u(\tau - s) \quad \text{(A2)}$$

with

$$K_3(s) = -\left[\frac{e^{z\omega_1 s}(\omega_3 - \omega_2) - e^{z\omega_2 s}(\omega_3 - \omega_1) + e^{z\omega_3 s}(\omega_2 - \omega_1)}{(\omega_2 - \omega_1)(\omega_3 - \omega_1)(\omega_3 - \omega_2)}\right] \quad \text{(A3)}$$

The time variable $\tau = t - t_0$ is a convenience which allows for an adjustable reference time t_0, and ω_1, ω_2, and ω_3 are the normal mode frequencies of the local-linear analogue which are the solutions of $(i\omega)^3 + \alpha_2(i\omega)^2 + \alpha_1(i\omega) + \alpha_0 = 0$. The quantity u represents the expansion in derivatives of the input data on the right side of (2).

$$u(\tau) = \sum_{n=0}^{l-1} \beta_n \frac{d^n I}{d\tau^n} \quad \text{(A4)}$$

Using the notation $c_1 = \exp(i\omega_1 \Delta t)$, $c_2 = \exp(i\omega_2 \Delta t)$, $c_3 = \exp(i\omega_3 \Delta t)$, $O(j) = O(t_0 + j\,\Delta t)$, and $S_3(j) = S_3(t_0 + j\,\Delta t)$, in which Δt is the time interval of the discrete data, (A1) yields

$$\begin{aligned} O(0) &= c_1 + c_2 + c_3 \\ O(1) &= c_1 c_1 + c_2 c_2 + c_3 c_3 + S_3(1) \\ O(2) &= c_1 c_1^2 + c_2 c_2^2 + c_3 c_3^2 + S_3(2) \\ O(3) &= c_1 c_1^3 + c_2 c_2^3 + c_3 c_3^3 + S_3(3) \end{aligned} \quad \text{(A5)}$$

The $O(j)$ in this last expression are set to the four consecutive values ($m = 3$) of output data that appear in (1). Then the continuous solution of (2) agrees with the output data in (1) at the discrete data times. We wish to solve the first three equations of (A5) for the coefficients c_1, c_2, and c_3, and substitute these solutions into the fourth equation to eliminate these coefficients from the system. A convenient way to do this is to note that $O(3) - S_3(3)$ must be found a linear combination of $O(2) - S_3(2)$, $O(1) - S_3(1)$, and $O(0)$. Thus

$$O(3) - S_3(3) = a[O(2) - S_3(2)] + b[O(1) - S_3(1)] + cO(0) \quad \text{(A6)}$$

in which a, b, and c depend only on c_1, c_2, and c_3. Substituting (A5) into (A6), and treating c_1, c_2, and c_3 as independent coefficients, we find

$$\begin{aligned} c_1^3 - ac_1^2 - bc_1 - c &= 0 \\ c_2^3 - ac_2^2 - bc_2 - c &= 0 \\ c_3^3 - ac_3^2 - bc_3 - c &= 0 \end{aligned} \quad \text{(A7)}$$

Suppose c is a solution of

$$(c - c_1)(c - c_2)(c - c_3) = c^3 - (c_1 + c_2 + c_3)c^2 + (c_1c_2 + c_1c_3 + c_2c_3)c - c_1c_2c_3 = 0 \quad \text{(A8)}$$

If the obvious solutions are inserted into this equation, then the identities

$$\begin{aligned} c_1^3 - (c_1 + c_2 + c_3)c_1^2 + (c_1c_2 + c_1c_3 + c_2c_3)c_1 - c_1c_2c_3 &= 0 \\ c_2^3 - (c_1 + c_2 + c_3)c_2^2 + (c_1c_2 + c_1c_3 + c_2c_3)c_2 - c_1c_2c_3 &= 0 \\ c_3^3 - (c_1 + c_2 + c_3)c_3^2 + (c_1c_2 + c_1c_3 + c_2c_3)c_3 - c_1c_2c_3 &= 0 \end{aligned} \quad \text{(A9)}$$

result. Comparing (A7) to (A9), we see that we must have $a = c_1 + c_2 + c_3$, $b = -(c_1c_2 + c_1c_3 + c_2c_3)$, and $c = c_1c_2c_3$. By substituting these expressions into (A6), and by using trapezoidal approximations to the integrals that appear in the $S_3(j)$, we find

$$\begin{aligned} O(3) &= A_0O(2) + A_1O(1) + A_2O(0) \\ &\quad + \Delta t\, K_3(\Delta t)\, u(2) \\ &\quad + \Delta t[K_3(2\Delta t) - (c_1 + c_2 + c_3)\, K_3(\Delta t)]\, u(1) \end{aligned} \quad \text{(A10)}$$

in which

$$\begin{aligned} A_0 &= (c_1 + c_2 + c_3) \\ A_1 &= -(c_1c_2 + c_1c_3 + c_2c_3) \\ A_2 &= c_1c_2c_3 \end{aligned} \quad \text{(A11)}$$

are to be identified with the local-linear filter coefficients in (1). At this point we introduce a polynomial fit of order $l - 1$ (linear in this case) to the input data in (1) to obtain

$$u(2) = \beta_0\, I(2) + \beta_1 \left[\frac{I(2) - I(1)}{\Delta t}\right] \quad \text{(A12)}$$

$$u(1) = \beta_0\, I(1) + \beta_1 \left[\frac{I(2) - I(1)}{\Delta t}\right] \quad \text{(A13)}$$

Substituting these expressions into (A10) and collecting terms, we find

$$\begin{aligned} O(3) &= A_0O(2) + A_1O(1) + A_2O(0) \\ &\quad + B_0I(2) + B_1I(1) \end{aligned} \quad \text{(A14)}$$

with

$$\beta_0 = \frac{B_0 + B_1}{\Delta t\,[K(1) + K(2) - (c_1 + c_2 + c_3)\, K(1)]} \quad \text{(A15)}$$

$$\beta_1 = \frac{[K_2 - (c_1 + c_2 + c_3)\, K(1)]\, B_0 - K(1)\, B_1}{[K(1) + K(2) - (c_1 + c_2 + c_3)\, K(1)]^2} \quad \text{(A16)}$$

At this point we have cast the solution of the local-linear analogue

(2), when evaluated at the times corresponding to the discrete input and output data, in the form of the local-linear predictor (1). Equations (A15) and (A16) give the β_n in terms of the B_n. It remains to find the values of the analogue coefficients α_n that are implied by this construct.

Equation (3) has poles on the complex q plane at the positions of the zeroes in the polynomial contained in its denominator. The positions of these zeroes are given by

$$q^3 - A_0 q^2 - A_1 q - A_2 =$$
$$q^3 - (q_1 + q_2 + q_3)q^2 + (q_1 q_2 + q_1 q_3 + q_2 q_3)q - q_1 q_2 q_3 = 0 \quad \text{(A17)}$$

We find these positions using a numerical root finder. Comparing (A17) with (A11), we find $c_1 = q_1$, $c_2 = q_2$, and $c_3 = q_3$, and thus c_1, c_2, and c_3 are fixed simultaneously, as are ω_1, ω_2, and ω_3. However, from (A1), these frequencies are the normal frequencies of the local-linear analogue which satisfy

$$\begin{aligned}(i\omega_1)^3 + \alpha_2(i\omega_1)^2 + \alpha_1(i\omega_1) + \alpha_0 = 0\\ (i\omega_2)^3 + \alpha_2(i\omega_2)^2 + \alpha_1(i\omega_2) + \alpha_0 = 0\\ (i\omega_3)^3 + \alpha_2(i\omega_3)^2 + \alpha_1(i\omega_3) + \alpha_0 = 0\end{aligned} \quad \text{(A18)}$$

Given the normal frequencies, this system can be inverted to find the analogue coefficients.

Thus we have completed the transformation of local-linear predictor (1) to local-linear analogue (2) for $m = 3$ and $l = 2$. This transformation has the property that the analogue solution agrees with the predictor data at the discrete data times in the predictor. This derivation removes the inconsistency in the related results of KEA. A review of this derivation will show that there is no step that cannot be carried to higher order in both m and l. As discussed above, for $m = 2$ we have extended this calculation to arbitrary l. Further extensions will be reported in the future.

Acknowledgments. We wish to thank Y Kamide and S. Sharma who provided the high time-resolution solar wind and *Dst* index data used in this study. This research was supported by the NASA grant NRA-94-SSM-SR&T-046.

The Editor thanks the referees for their assistance in evaluating this paper.

References

Burton, R. K., R L. McPherron, and C T. Russell, An empirical relationship between interplanetary conditions and Dst, *J. Geophys Res*, *80*(31), 4204, 1975.

Feldstein, Y. I., Modelling of the magnetic field of magnetospheric ring current as a function of interplanetary medium parameters, *Space Sci. Rev.*, *59*(83), 83–165, 1992.

Golub, G H., and C F Van Loan, *Matrix Computations*, 3rd ed., Johns Hopkins Univ. Press, Baltimore, Md., 1996.

Gonzalez, W. D , and B. T. Tsurutani, Criteria of interplanetary parameters causing intense magnetic storms (*Dst* < -100 nT), *Planet. Space Sci.*, *35*(9), 1101–1109, 1987.

Hunter, N. F, and J. Theiler, Characterization of nonlinear input-output systems using time series analysis, in *Proceedings of the 1st Experimental Chaos Conference*, edited by S. Vohora, M Spano, M Schlesinger, L. Pecora, and W. Ditto, p. 54, World Sci., River Edge, N. J., 1992.

Klimas, A. J., D Vassiliadis, and D. N. Baker, Data-derived analogues of the magnetospheric dynamics, *J Geophys. Res.*, *102*, 26,993, 1997.

Press, W. H., B. P. Flannery, S. A. Teukolsky, and W. T. Vettering, *Numerical recipes, the Art of Scientific Computing (FORTRAN Version)*, Cambridge Univ Press, New York, 1992.

Valdivia, J. A., A. S. Sharma, and K. Papadopoulos, Prediction of magnetic storms by nonlinear dynamical methods, *Geophys. Res. Lett.*, *23*, 2899, 1996.

Vassiliadis, D , A. J. Klimas, D. N. Baker, and D. A. Roberts, A description of solar wind-magnetosphere coupling based on nonlinear filters, *J. Geophys Res.*, *100*, 3495, 1995.

Vassiliadis, D., V Angelopoulos, D. N. Baker, and A. J. Klimas, The relationship between the northern polar cap and auroral electrojet geomagnetic indices in the wintertime, *Geophys. Res. Lett.*, *23*, 2781, 1996.

D N. Baker, Laboratory for Atmospheric and Space Physics, University of Colorado, Boulder, CO 80309. (e-mail: baker@lynx.colorado.edu)

A. J. Klimas, NASA Goddard Space Flight Center, Greenbelt, MD 20771. (e-mail: alex.klimas@gsfc.nasa.gov)

D. Vassiliadis, Universities Space Research Associates, Seabrook, MD 20706. (e-mail: vassi@lepgst.gsfc.nasa.gov)

(Received January 27, 1998; revised April 22, 1998; accepted May 6, 1998.)